VNU Journal of Science: Mathematics - Physics
Journal homepage: https://js.vnu.edu.vn/MaP

Original Article

# Elastic Deformation and Elastic Wave Velocity for Cubic Metal and Binary Interstitial Alloy's Thin Films at Different Temperatures, Pressures, Interstitial Atomic Concentrations and Film Thicknesses

Nguyen Quang Hoc[1,*], Hua Xuan Dat[1], Phan Minh Hang[1], Le Hong Viet[2], Doan Quang Tuan[3], Quach Si Gia Khoa[4]

[1]*Hanoi National University of Education, 136 Xuan Thuy, Cau Giay, Hanoi, Vietnam*
[2]*Tran Quoc Tuan University, Co Dong, Son Tay, Hanoi, Vietnam*
[3]*Hanoi-Amsterdam High School, 1 Hoang Minh Giam, Cau Giay, Hanoi, Vietnam*
[4]*VNU University of Science, 334 Nguyen Trai, Thanh Xuan, Hanoi, Vietnam*

Received 01 February 2024
Revised 27 June 2024; Accepted 25 July 2024

**Abstract:** The theory of elastic deformation and elastic wave for cubic metal and binary interstitial alloy's thin films is builded by a statistical moment method (SMM). The obtained results have been applied to perform numerical calculations for W, Au, WSi and AuSi materials. Some SMM calculations for W, Au are compared with experiments and other calculation methods. Other SMM calculations are new and predict experimental results.

*Keywords:* Binary interstitial alloy, thin film, elastic deformation, elastic wave velocity, SMM

## 1. Introduction

Statistical moment method (SMM) has been applied to study the elastic deformation and elastic wave velocity of bulk metals, interstitial alloys [1-7] and the thermodynamic properties of metal films [8-10].

* Corresponding author.
*E-mail address:* hocnq@hnue.edu.vn

https//doi.org/10.25073/2588-1124/vnumap.4917

Researchers are often interested in stand-mounted films. The average values of the Young's moduli are calculated for Ag, Cu, Al and Ag/Cu multilayers [11]. The biaxial elastic modulus of the $\alpha$ phase agreed with results of bulk $\alpha$ tantalum [12]. Young modulus of nanostructured metallic films is measured by experiments [13]. The tensile tests were applied for the freestanding foils and wires [14]. Cu, Ni and Pd layers were deposited on Si wafer substrates by DC-magnetron sputtering. The mechanical stresses were studied by X-ray diffraction measurements [15]. A novel theory predicted the growth mode of a metallic film on an insulating substrate [16]. Studies on mechanical properties of thin films, especially free metal films, are quite limited.

Recently, many mechanical properties of metals and alloy's films have attracted the attention of researchers [8-10, 17-18]. W and WSi are materials having very high melting points [19, 20]. Au and AuSi have many applications [21]. AuSi has long attracted the interest of researchers due to its applications and unusual physical properties. The Young's modulus of Au-3%Si alloy was considered in [22]. Au is often used to make jewelry. According to research [23], AuSi alloy has a color similar to Au and Au alloys can be produced with Si concentrations of 2.5, 2.8 and 3.0%. The hardness of AuSi is about 110 HV and is greater than that of traditional high-purity gold alloys. The temperature dependence of the Young's modulus for Au at zero pressure and in the temperature range from 0 to 1100K has been determined by calculations [24-26] and measured by experiments [27]. The dependence of the volume ratio ($V$ is the volume at pressure $P$ and $V_0$ is the volume at zero pressure) on pressure for Au at room temperature and in the pressure range from 0 to 1,000 GPa is shown in [24, 28-30]. The pressure dependence of the elastic constant $C_{44}$ in the pressure range from 0 to 100 GPa for Au at room temperature is determined by experiments [31-34]. In this work, we introduce the theory of elastic deformation and elastic wave velocity for cubic binary interstitial alloy's film based on SMM [1-6, 8-10, 17, 21, 35]. The numerical calculations are caried out for films of W, Au, WSi and AuSi.

## 2. Analytic Calculations

Assume a free thin film of a cubic interstitial alloy AB consisting $n^*$ layers (two outer layers, two next outer layers and $n^*-4$ inner layers) with thickness $d$. The number of atoms of these layers respectively are of $N^{ol}$, $N^{nol}$ and $N^{\mathrm{il}}$ [8-10].

A is the atom in pure metal A, $A_1$ is the main metal atom A at body center (or face center), $A_2$ is the main metal atom A at vertices and B is the interstitial atom at face center (or body center) of cubic unit cell. For the layer $\mathrm{l}$ (the inner layer or the next outer layer), the displacement of the atom X (X = A, $A_1$, $A_2$, B) at pressure $P$ and temperature $T$ from the equilibrium position has the form [6, 8, 35]

$$y_X^{\mathrm{l}} = \sqrt{\frac{2\gamma_X^{\mathrm{l}}\theta^2}{3\left(k_X^{\mathrm{l}}\right)^3}A_X^{\mathrm{l}}}\,,\ A_X^{\mathrm{l}} \equiv a_{1X}^{\mathrm{l}} + \sum_{i=2}^{6}\left(\frac{\gamma_X^{\mathrm{l}}\theta}{\left(k_X^{\mathrm{l}}\right)^2}\right)^i a_{iX}^{\mathrm{l}}\,, \tag{1}$$

where $\theta = k_{\mathrm{Bo}}T, k_{\mathrm{Bo}}$ is the Boltzmann constant, $T$ is the absolute temperature, $y_X^{\mathrm{l}} \equiv y_X^{\mathrm{l}}(P,T)$, $k_X^{\mathrm{l}}$ and $\gamma_X^{\mathrm{l}}$ are the harmonic and anharmonic crystal parameters of the atom X in the layer $\mathrm{l}$ and are determined from the nearest neighbor distance $r_{1X}^{\mathrm{l}}(P,0)$ between two atoms at pressure $P$ and temperature $T$ = 0K in the layer $\mathrm{l}$ and $r_{1X}^{\mathrm{l}}(P,0)$ is calculated from the equation of state [35]

$$Pv_X^{\mathrm{l}} = -r_{1X}^{\mathrm{l}}\left(\frac{1}{6}\frac{\partial u_{0X}^{\mathrm{l}}}{\partial r_{1X}^{\mathrm{l}}} + \frac{\mathrm{h}\omega_X^{\mathrm{l}}}{4k_X^{\mathrm{l}}}\frac{\partial k_X^{\mathrm{l}}}{\partial r_{1X}^{\mathrm{l}}}\right), \tag{2}$$

$u_{0X}^{\mathrm{l}}$ is the cohesive energy, $v_X^{\mathrm{l}} = \frac{4r_{1X}^{\mathrm{l}3}}{3\sqrt{3}}$ is the volume of cubic unit cell for BCC lattice, $v_X^{\mathrm{l}} = \frac{r_{1X}^{\mathrm{l}3}}{\sqrt{2}}$ is the volume of cubic unit cell for FCC lattice, $m_X^{\mathrm{l}}$ is the mass for the atom X in the layer $\mathrm{l}$ and $a_{1X}^{\mathrm{l}}$ are complex functions of $Y_X^{\mathrm{l}} \equiv x_X^{\mathrm{l}} \coth x_X^{\mathrm{l}}$.

For the outer layer [6, 8, 35],

$$y_X^{ol} = -\frac{\gamma_X^{ol}\theta}{\left(k_X^{ol}\right)^2} Y_X^{ol}, \quad Y_X^{ol} \equiv x_X^{ol} \coth x_X^{ol}, \tag{3}$$

where $k_X^{ol}, \gamma_X^{ol}, x_X^{ol}$ are determined in the same way as above.

For the layer *m* (the inner layer, the next outer layer or the outer layer) [6, 8, 35],

$$r_{1B}^m(P,T) = r_{1B}^m(P,0) + y_{A_1}^m(P,T), r_{1A}^m(P,T) = r_{1A}^m(P,0) + y_A^m(P,T),$$

$$r_{1A_1}^m(P,T) = r_{1B}^m(P,T),\ r_{1A_2}^m(P,T) = r_{1A_2}^m(P,0) + y_B^m(P,T). \tag{4}$$

The mean nearest neighbor distance $\overline{r_{1A}^m(P,T)}$ between two atoms A in the layer *m* is determined by [6]

$$\overline{r_{1A}^m(P,T)} = \overline{r_{1A}^m(P,0)} + \overline{y^m(P,T)}, \overline{r_{1A}^m(P,0)} = \left(1 - c_B^m\right) r_{1A}^m(P,0) + c_B^m r_{1A}'^m(P,0),$$

$$\overline{y^m(P,T)} = \sum_X c_X^m y_X^m(P,T), \tag{5}$$

where $r_{1A}'^m(P,0) = \sqrt{3} r_{1B}^m(P,0),\ c_A^m = 1 - 7c_B^m, c_{A_1}^m = 2c_B^m, c_{A_2}^m = 4c_B^m$ for BCC lattice $r_{1A}'^m(P,0) = \sqrt{2} r_{1B}^m(P,0),\ c_A^m = 1 - 15c_B^m, c_{A_1}^m = 6c_B^m, c_{A_2}^m = 8c_B^m$ for FCC lattice, $c_X^m = \frac{N_X^m}{N^m}$ is the concentration of atoms X in the layer *m*, $N_X^m$ is the the number of atoms X in the layer *m* and $N^m$ is the number of atoms in the layer *m*.

The Helmholtz free energy for the layer $\mathrm{l}$ of alloy film has the form [6, 35]

$$\Psi^{\mathrm{l}} = N^{\mathrm{l}} \left( \sum_X c_X^{\mathrm{l}} \psi_X^{\mathrm{l}} - T S_c^{\mathrm{l}} \right),$$

$$\Psi_X^{\mathrm{l}} = N^{\mathrm{l}} \psi_X^{\mathrm{l}} \approx U_{0X}^{\mathrm{l}} + 3N^{\mathrm{l}} \theta [x_X^{\mathrm{l}} + \ln(1 - e^{-2x_X^{\mathrm{l}}})] +$$

$$+ \frac{3N^{\mathrm{l}}\theta^2}{\left(k_X^{\mathrm{l}}\right)^2} \left[ \gamma_{2X}^{\mathrm{l}} \left(Y_X^{\mathrm{l}}\right)^2 - \frac{2\gamma_{1X}^{\mathrm{l}}}{3} \left(1 + \frac{Y_X^{\mathrm{l}}}{2}\right) \right] +$$

$$+ \frac{6N^{\mathrm{l}}\theta^3}{\left(k_X^{\mathrm{l}}\right)^4} \left[ \frac{4}{3} \left(\gamma_{2X}^{\mathrm{l}}\right)^2 \left(1 + \frac{Y_X^{\mathrm{l}}}{2}\right) Y_X^{\mathrm{l}} - 2\left( \left(\gamma_{1X}^{\mathrm{l}}\right)^2 + 2\gamma_{1X}^{\mathrm{l}} \gamma_{2X}^{\mathrm{l}} \right) \left(1 + \frac{Y_X^{\mathrm{l}}}{2}\right) \left(1 + Y_X^{\mathrm{l}}\right) \right]. \tag{6}$$

The Helmholtz free energy of the outer layer has the form [6, 35]

$$\Psi^{ol} = N^{ol} \left( \sum_X c_X^{ol} \psi_X^{ol} - T S_c^{ol} \right),$$

$$\Psi_X^{ol} = N^{ol}\psi_X^{ol} \approx U_0^{ol} + 3N^{ol}\theta[x_X^{ol} + \ln(1-e^{-2x_X^{ol}})]. \quad (7)$$

In Eqs. (6) and (7), $U_{0X}^m = \frac{N^m}{2}u_{0X}^m$, $\psi_X^m$ is the Helmholtz free energy of an atom X in the layer *m* and $S_c^m$ is the configurational entropy of the alloy in the layer *m*.

The Helmholtz free energies of the layer *m* in the harmonic approximation have the form [6, 8, 35]

$$\Psi^m = N^m\left(\sum_X c_X^m\psi_X^m - TS_c^m\right),$$

$$\Psi_X^m = N^m\psi_X^m \approx U_0^m + 3N^m\theta[x_X^m + \ln(1-e^{-2x_X^m})]. \quad (8)$$

The Helmholtz free energies for an atom of the BCC and FCC films respectively have the form [8]

$$\frac{\Psi}{N} = \frac{d\sqrt{3}-3\bar{a}}{d\sqrt{3}+\bar{a}}\psi^{tr} + \frac{2\bar{a}}{d\sqrt{3}+\bar{a}}\psi^{ng} + \frac{2\bar{a}}{d\sqrt{3}+\bar{a}}\psi^{ng1} - \frac{TS_c}{N} =$$
$$= \frac{d\sqrt{3}-3\bar{a}}{d\sqrt{3}+\bar{a}}\left(\sum_X c_X^{tr}\psi_X^{tr} - TS_c^{tr}\right) + \frac{2\bar{a}}{d\sqrt{3}+\bar{a}}\left(\sum_X c_X^{ng}\psi_X^{ng} - TS_c^{ng}\right) +$$
$$+ \frac{2\bar{a}}{d\sqrt{3}+\bar{a}}\left(\sum_X c_X^{ng1}\psi_X^{ng1} - TS_c^{ng1}\right) - \frac{TS_c}{N}, \quad (9)$$

$$\frac{\Psi}{N} = \frac{d\sqrt{2}-3\bar{a}}{d\sqrt{2}+\bar{a}}\psi^{il} + \frac{2\bar{a}}{d\sqrt{2}+\bar{a}}\psi^{ol} + \frac{2\bar{a}}{d\sqrt{2}+\bar{a}}\psi^{nol} - \frac{TS_c}{N} =$$
$$= \frac{d\sqrt{2}-3\bar{a}}{d\sqrt{2}+\bar{a}}\left(\sum_X c_X^{il}\psi_X^{il} - TS_c^{il}\right) + \frac{2\bar{a}}{d\sqrt{2}+\bar{a}}\left(\sum_X c_X^{ol}\psi_X^{ol} - TS_c^{ol}\right) +$$
$$+ \frac{2\bar{a}}{d\sqrt{2}+\bar{a}}\left(\sum_X c_X^{nol}\psi_X^{nol} - TS_c^{nol}\right) - \frac{TS_c}{N}, \quad (10)$$

where $N = N^{il} + N^{nol} + N^{ol}$, $S_c$ is the configurational entropy of the film, $\psi^{il}, \psi^{nol}, \psi^{ol}$ respectively are the Helmholtz free energies of an atom in the inner layer, the next outer layer and the outer layer of the film, $\bar{a}$ is the mean nearest neighbor distance between two atoms, $\bar{b}$ is the average thickness of the two respective layers and $\bar{a}_c$ is the average lattice constant of the film

For body-centered cube (BCC) film [8],

$$\bar{b} = \frac{\bar{a}}{\sqrt{3}},\ \bar{a}_c = 2\bar{b} = \frac{2\bar{a}}{\sqrt{3}}.\quad n^* = 1 + \frac{d\sqrt{3}}{\bar{a}}. \quad (11)$$

For face- centered cube (FCC) film [8],

$$\bar{b} = \frac{\bar{a}}{\sqrt{2}},\ \bar{a}_c = 2\bar{b} = \sqrt{2}\bar{a},\ \ n^* = 1 + \frac{d\sqrt{2}}{\bar{a}}. \quad (12)$$

The Young moduli of the BCC and FCC films have the form [1, 6]

$$E_{YAB} = \frac{d\sqrt{3}-3\bar{a}}{d\sqrt{3}+\bar{a}} E_Y^{il} + \frac{2\bar{a}}{d\sqrt{3}+\bar{a}} E_Y^{ol} + \frac{2\bar{a}}{d\sqrt{3}+\bar{a}} E_Y^{nol}, \quad (13)$$

$$E_{YAB} = \frac{d\sqrt{2}-3\bar{a}}{d\sqrt{2}+\bar{a}} E_Y^{il} + \frac{2\bar{a}}{d\sqrt{2}+\bar{a}} E_Y^{ol} + \frac{2\bar{a}}{d\sqrt{2}+\bar{a}} E_Y^{nol}, \quad (14)$$

where

$$E_Y^m = \sum_X c_X E_{YX}^m,\ E_{YX}^m = \frac{1}{\pi\left(r_{01X}^m + y_X^m\right)A_{1X}^m}, A_{1X}^m = \frac{1}{k_X^m}\left[1+\frac{2\left(\gamma_X^m\right)^2\theta^2}{\left(k_X^m\right)^4}\left(1+\frac{Y_X^m}{2}\right)\left(1+Y_X^m\right)\right]. \quad (15)$$

The bulk modulus, the shearing modulus, the elastic constants, the longitudinal wave velocity and the tranverse wave velocity of the film respectively are given by [1, 6]

$$K_{AB} = \frac{E_{YAB}}{3(1-2\nu_{AB})},\ G_{AB} = \frac{E_{YAB}}{2(1+\nu_{AB})}, \quad (16)$$

$$C_{11AB} = \frac{E_{YAB}(1-\nu_{AB})}{(1+\nu_{AB})(1-2\nu_{AB})}, C_{12AB} = \frac{E_{YAB}\nu_{AB}}{(1+\nu_{AB})(1-2\nu_{AB})}, C_{44AB} = \frac{E_{YAB}}{2(1+\nu_{AB})}, \quad (17)$$

$$V_{ABd} = \sqrt{\frac{2C_{44AB}+C_{12AB}}{\rho_{AB}}}, V_{ABn} = \sqrt{\frac{C_{44AB}}{\rho_{AB}}}, \quad (18)$$

where

$$\nu_{AB} = c_A\nu_A + c_B\nu_B \approx \nu_A, \quad (20)$$

$\nu_{AB}$ is the Poisson ratio of the alloy film AB, $\nu_A$, $\nu_B$ are the Poisson ratios of materials A and B. Because $c_B \ll c_A$ then $\nu_{AB} \approx \nu_A$. $\rho_{AB} = \frac{m_{AB}}{V_{AB}} \approx \rho_A, V_{AB} = N v_{AB}$, $\rho_{AB}$ is the density of the alloy film AB, $\rho_A$ is the density of the main metal A and $V_{AB}$ is the volume of the alloy film AB.

The cohesive energy $u_0$ and crystal parameters $k$, $\gamma_1, \gamma_2, \gamma$ for the atom B in the approximation of two coordination spheres, the atoms $A_1$ and $A_2$ in the approximation of three coordination spheres for the inner layer of the film have the form as in bulk material for BCC lattice [6, 8, 35] and for FCC lattice [36].

The cohesive energy $u_0$ and crystal parameters $k$, $\gamma_1, \gamma_2, \gamma$ for the atom B in the approximation of two coordination spheres, the atoms $A_1$ and $A_2$ in the approximation of three coordination spheres for the next outer layer (there is a vacancy on the z-axis in the second coordination sphere taking $u_0$, $k$, $\gamma_1, \gamma_2, \gamma$ of the atom B and in the third coordination sphere taking taking $u_0$ $\gamma_1, \gamma_2, \gamma$ of the atoms $A_1$ and $A_2$) of the film for FCC lattice have the form as in [36] and for BCC lattice have the form as in [6, 8, 35].

The cohesive energy $u_0$ and crystal parameters $k$, $\gamma_1, \gamma_2, \gamma$ for the atom B in the approximation of two coordination spheres, the atoms $A_1$ and $A_2$ in the approximation of three coordination spheres for the outer layer (remove an atom on the second coordination sphere taking $u_0$, $k$, $\gamma_1, \gamma_2, \gamma$ of the atom

B and on the third coordination sphere taking taking $u_0\ \gamma_1, \gamma_2, \gamma$ of the atoms $A_1$ and $A_2$) of the film for FCC lattice have the form as in [7] and for BCC lattice have the form as in [6, 8, 35].

When thickness *d* of the thin film is large enough, the theory of elastic deformation and elastic wave velocity for the cubic interstititial alloy AB's film becomes that for the cubic interstititial alloy AB. When the interstitial atom concentration is zero, the theory of elastic deformation and elastic wave velocity for the cubic interstititial alloy AB's film becomes that for the cubic main metal A's film.

We perform numerical calculations according to above mentioned theory for W, Au, WSi and AuSi in section 3.

## 3. Numerial Calculations and Discussions for W, Au, WSi and AuSi

For interactions W-W, Au-Au, Si-Si in W, Au, WSi and AuSi, we use the Mie-Lennard-Jones potential [37]

$$\varphi(r) = \frac{D}{n-m}\left[ m\left(\frac{r_0}{r}\right)^n - n\left(\frac{r_0}{r}\right)^m \right], \tag{21}$$

where the potential parameters $D, r_0, m, n$ are given in Table 1. We use the following approximations

$$\varphi_{\text{W-Si}} \approx \frac{1}{2}\left(\varphi_{\text{W-W}} + \varphi_{\text{Si-Si}}\right), \varphi_{\text{Au-Si}} \approx \frac{1}{2}\left(\varphi_{\text{Au-Au}} + \varphi_{\text{Si-Si}}\right). \tag{22}$$

Table 1. The parameters $D, r_0, m, n$ of the Mie-Lennard-Jones potential [23]

| Interaction | m | n | $D(10^{-16}\text{erg})$ | $r_0(10^{-10}\text{m})$ |
|---|---|---|---|---|
| W-W [37] | 6.5 | 10.5 | 15564.744 | 2.7365 |
| Au-Au [37] | 5.5 | 10.5 | 4683 | 2.8751 |
| Si-Si [37] | 6.0 | 12.0 | 45128.24 | 2.295 |

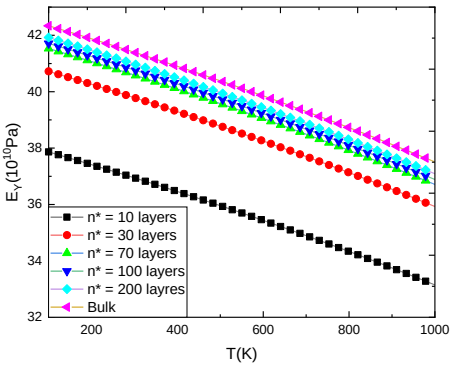


Figure 1. $E_Y(T, n^*)$ for W at $P = 0$ calculated by SMM.

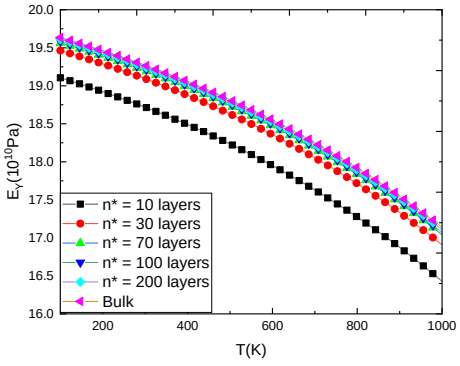


Figure 2. $E_Y(T, n^*)$ for WSi at $c_{\text{Si}} = 5\%$, $P = 0$ calculated by SMM.

The temperature and layer number dependences of Young modulus for W and Au at $P = 0$ calculated by SMM are shown in Figs. 1 and 5. The temperature and layer number dependences of Young modulus for WSi and AuSi at $c_{Si} = 5\%$, $P = 0$ calculated by SMM are shown in Figs. 2 and 6. The pressure and layer number dependences of Young modulus for W and Au at $T = 300$K calculated by SMM are shown in Figs. 3 and 7. The pressure and layer number dependences of Young modulus for WSi and AuSi at $c_{Si} = 5\%$, $T = 300$K calculated by SMM are shown in Figs. 4 and 8.

The nearest neighbor distance of a film strongly depends on thickness, temperature and pressure. This distance increases with the increase of thickness, increases sharply with the increase of temperature and decreases with the increase of pressure. As the number of layers increases until about 200 layers (about 35 nm thickness), elastic deformation and elastic wave velocity quantities of the film approach the values of bulk material.

Silicon concentration and layer number dependences of nearest neighbor distance and mean nearest neighbor $a$, elastic moduli $E_Y$, $K$, $G$, elastic constants $C_{11}$, $C_{12}$, $C_{44}$, longitudinal velocity $V_l$ and transverse $V_t$ for films W, Au,WSi and AuSi at $P = 0$, $T = 300$K calculated by SMM are summarised in Tables 2 and 3. Pressure and layer number dependences of longitudinal velocity and transsverse velocity for Au at $T = 300$K calculated by SMM are summarised in Table 4.

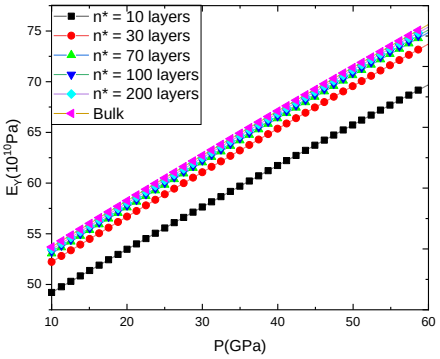


Figure 3. $E_Y(P, n^*)$ for W at $T = 300$K calculated by SMM.

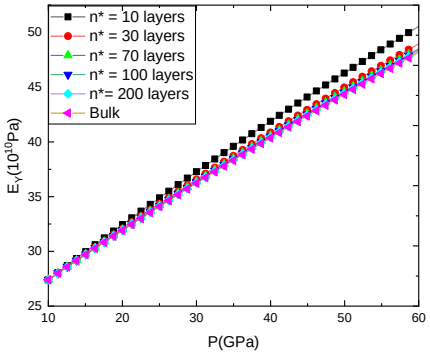


Figure 4. $E_Y(P, n^*)$ for WSi at $c_{Si} = 5\%$, $T = 300$K calculated by SMM.

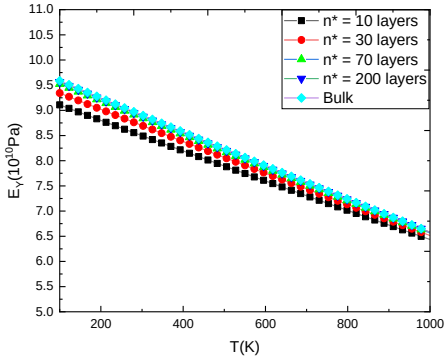


Figure 5. $E_Y(T, n^*)$ for Au at $P = 0$ calculated by SMM.

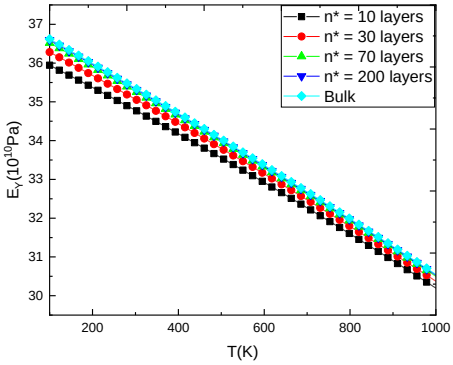


Figure 6. $E_Y(T, n^*)$ for AuSi at $c_{Si} = 5\%$, $P = 0$ calculated by SMM.

Table 2. $a(c_{Si}, n^*)$, $E_Y(c_{Si}, n^*)$, $K(c_{Si}, n^*)$, $G(c_{Si}, n^*)$, $C_{11}(c_{Si}, n^*)$, $C_{12}(c_{Si}, n^*)$, $C_{44}(c_{Si}, n^*)$, $V_l$ $(c_{Si}, n^*)$ and $V_t$ $(c_{Si}, n^*)$ for films W and WSi at $P = 0$, $T = 300$K calculated by SMM

| Layer number | $c_{Si}$(%) | 0 | 1 | 3 | 5 |
|---|---|---|---|---|---|
| | $a(10^{-10}\text{m})$ | 2.642 | 2.658 | 2.690 | 2.722 |
| | $E_Y(10^{10}\text{Pa})$ | 38.76 | 33.91 | 25.81 | 19.47 |
| | $G(10^{10}\text{Pa})$ | 29.36 | 25.88 | 19.99 | 15.31 |
| 10 | $K(10^{10}\text{Pa})$ | 15.14 | 13.23 | 10.05 | 7.56 |
| | $C_{11}(10^{10}\text{Pa})$ | 4.96 | 4.35 | 3.34 | 2.54 |
| | $C_{12}(10^{10}\text{Pa})$ | 1.93 | 1.71 | 1.33 | 1.03 |
| | $C_{44}(10^{10}\text{Pa})$ | 1.51 | 1.32 | 1.00 | 0.76 |
| | $V_t$ $(10^5\text{cm/s})$ | 4.69 | 4.39 | 3.85 | 3.35 |
| | $V_l$ $(10^5\text{cm/s})$ | 2.59 | 2.42 | 2.11 | 1.83 |
| | $a(10^{-10}\text{m})$ | 2.649 | 2.665 | 2.697 | 2.730 |
| | $E_Y(10^{10}\text{Pa})$ | 40.85 | 35.34 | 26.28 | 19.32 |
| | $G(10^{10}\text{Pa})$ | 30.95 | 26.97 | 20.35 | 15.18 |
| 70 | $K(10^{10}\text{Pa})$ | 15.96 | 13.79 | 10.23 | 7.50 |
| | $C_{11}(10^{10}\text{Pa})$ | 5.22 | 4.54 | 3.40 | 2.52 |
| | $C_{12}(10^{10}\text{Pa})$ | 2.03 | 1.78 | 1.35 | 1.02 |
| | $C_{44}(10^{10}\text{Pa})$ | 1.60 | 1.38 | 1.02 | 0.75 |
| | $V_t$ $(10^5\text{cm/s})$ | 4.81 | 4.48 | 3.88 | 3.34 |
| | $V_l$ $(10^5\text{cm/s})$ | 2.66 | 2.47 | 2.13 | 1.82 |
| | $a(10^{-10}\text{m})$ | 2.649 | 2.666 | 2.698 | 2.731 |
| | $E_Y(10^{10}\text{Pa})$ | 41.07 | 35.50 | 26.32 | 19.30 |
| | $G(10^{10}\text{Pa})$ | 31.11 | 27.09 | 20.39 | 15.17 |
| 200 | $K(10^{10}\text{Pa})$ | 16.04 | 13.85 | 10.24 | 7.49 |
| | $C_{11}(10^{10}\text{Pa})$ | 5.25 | 4.56 | 3.40 | 2.52 |
| | $C_{12}(10^{10}\text{Pa})$ | 2.04 | 1.79 | 1.36 | 1.02 |
| | $C_{44}(10^{10}\text{Pa})$ | 1.60 | 1.38 | 1.02 | 0.75 |
| | $V_t$ $(10^5\text{cm/s})$ | 4.82 | 4.49 | 3.88 | 3.34 |
| | $V_l$ $(10^5\text{cm/s})$ | 2.67 | 2.48 | 2.13 | 1.82 |
| | $a(10^{-10}\text{m})$ | 2.649 | 2.666 | 2.698 | 2.731 |
| | $E_Y(10^{10}\text{Pa})$ | 41.19 | 35.57 | 26.35 | 19.29 |
| | $G(10^{10}\text{Pa})$ | 31.20 | 27.15 | 20.67 | 15.22 |
| Bulk | $K(10^{10}\text{Pa})$ | 16.09 | 13.88 | 10.23 | 7.483 |
| | $C_{11}(10^{10}\text{Pa})$ | 5.26 | 4.56 | 3.43 | 2.52 |
| | $C_{12}(10^{10}\text{Pa})$ | 2.05 | 1.78 | 1.38 | 1.02 |
| | $C_{44}(10^{10}\text{Pa})$ | 1.61 | 1.39 | 1.02 | 0.74 |
| | $V_t$ $(10^5\text{cm/s})$ | 4.83 | 4.49 | 3.89 | 3.34 |
| | $V_l$ $(10^5\text{cm/s})$ | 2.67 | 2.47 | 2.13 | 1.82 |

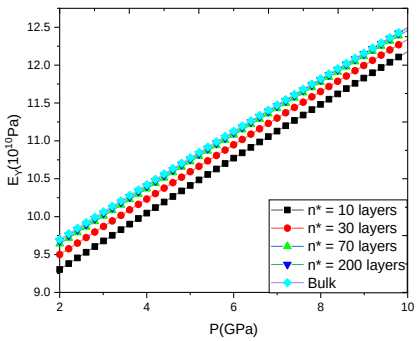


Figure 7. $E_Y(P, n^*)$ for Au at $T$ = 300K calculated by SMM.

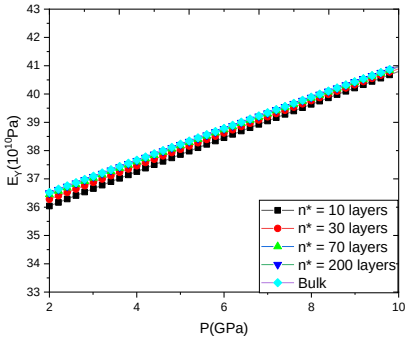


Figure 8. $E_Y(P, n^*)$ for AuSi at $c_{Si}$ = 5%, $T$ = 300K calculated by SMM.

Table 3. $a(c_{Si}, n^*)$, $E_Y(c_{Si}, n^*)$, $K(c_{Si}, n^*)$, $G(c_{Si}, n^*)$, $C_{11}(c_{Si}, n^*)$, $C_{12}(c_{Si}, n^*)$, $C_{44}(c_{Si}, n^*)$, $V_l\ (c_{Si}, n^*)$ and $V_t\ (c_{Si}, n^*)$ for films Au and AuSi at $P$ = 0, $T$ = 300K calculated by SMM

| Layer number | $c_{Si}$(%) | 0 | 1 | 3 | 5 |
|---|---|---|---|---|---|
| | $a(10^{-10}\text{m})$ | 2.84 | 2.85 | 2.86 | 2.87 |
| | $E_Y(10^{10}\text{Pa})$ | 8.54 | 13.79 | 24.29 | 34.79 |
| | $G(10^{10}\text{Pa})$ | 14.24 | 22.71 | 39.08 | 54.70 |
| 10 | $K(10^{10}\text{Pa})$ | 3.05 | 4.93 | 8.70 | 12.48 |
| | $C_{11}(10^{10}\text{Pa})$ | 18.31 | 29.29 | 50.68 | 71.34 |
| | $C_{12}(10^{10}\text{Pa})$ | 12.20 | 19.43 | 33.28 | 46.38 |
| | $C_{44}(10^{10}\text{Pa})$ | 3.05 | 4.93 | 8.70 | 12.48 |
| | $V_t\ (10^5\text{cm/s})$ | 3.08 | 3.90 | 5.12 | 6.08 |
| | $V_l\ (10^5\text{cm/s})$ | 1.26 | 1.60 | 2.12 | 2.54 |
| | $a(10^{-10}\text{m})$ | 2.85 | 2.85 | 2.86 | 2.87 |
| | $E_Y(10^{10}\text{Pa})$ | 8.90 | 14.17 | 24.72 | 35.27 |
| | $G(10^{10}\text{Pa})$ | 14.83 | 23.34 | 39.77 | 55.46 |
| 70 | $K(10^{10}\text{Pa})$ | 3.18 | 5.07 | 8.85 | 12.65 |
| | $C_{11}(10^{10}\text{Pa})$ | 19.07 | 30.10 | 51.58 | 72.33 |
| | $C_{12}(10^{10}\text{Pa})$ | 12.71 | 19.96 | 33.87 | 4.03 |
| | $C_{44}(10^{10}\text{Pa})$ | 3.18 | 5.07 | 8.85 | 12.65 |
| | $V_t\ (10^5\text{cm/s})$ | 3.14 | 3.95 | 5.17 | 6.12 |
| | $V_l\ (10^5\text{cm/s})$ | 1.28 | 1.62 | 2.14 | 2.56 |
| | $a(10^{-10}\text{m})$ | 2.85 | 2.85 | 2.86 | 2.87 |
| | $E_Y(10^{10}\text{Pa})$ | 8.94 | 1.21 | 24.77 | 35.33 |
| | $G(10^{10}\text{Pa})$ | 14.89 | 23.41 | 39.85 | 55.54 |
| 200 | $K(10^{10}\text{Pa})$ | 3.19 | 5.08 | 8.87 | 12.67 |
| | $C_{11}(10^{10}\text{Pa})$ | 19.15 | 30.18 | 51.67 | 72.44 |
| | $C_{12}(10^{10}\text{Pa})$ | 12.77 | 20.02 | 33.94 | 47.10 |

| | | | | | |
|---|---|---|---|---|---|
| | $C_{44}$($10^{10}$Pa) | 3.19 | 5.08 | 8.87 | 12.67 |
| | $V_t$ ($10^5$cm/s) | 3.15 | 3.95 | 5.17 | 6.13 |
| | $V_l$ ($10^5$cm/s) | 1.29 | 1.62 | 2.14 | 2.56 |
| | $a$($10^{-10}$m) | 2.85 | 2.85 | 2.86 | 2.87 |
| | $E_Y$($10^{10}$Pa) | 8.96 | 14.24 | 24.80 | 35.35 |
| | $G$($10^{10}$Pa) | 14.93 | 23.45 | 39.89 | 55.59 |
| Bulk | $K$($10^{10}$Pa) | 3.20 | 5.09 | 8.88 | 12.68 |
| | $C_{11}$($10^{10}$Pa) | 19.19 | 30.23 | 51.73 | 72.49 |
| | $C_{12}$($10^{10}$Pa) | 12.80 | 20.05 | 33.97 | 47.13 |
| | $C_{44}$($10^{10}$Pa) | 3.20 | 5.09 | 8.88 | 12.68 |
| | $V_t$ ($10^5$cm/s) | 3.15 | 3.96 | 5.18 | 6.13 |
| | $V_l$ ($10^5$cm/s) | 1.29 | 1.62 | 2.14 | 2.56 |

Table 4. $V_l$ $(P, n^*)$ and $V_t$ $(P, n^*)$ for Au at $T$ = 300K calculated by SMM

| | Layer number | 10 GPa | 20 GPa | 30 GPa | 40 GPa | 50 GPa |
|---|---|---|---|---|---|---|
| $V_l$ ($10^5$cm/s) | 10 | 3.21 | 3.34 | 3.46 | 3.57 | 3.68 |
| | 30 | 3.25 | 3.37 | 3.49 | 3.60 | 3.70 |
| | 70 | 3.27 | 3.39 | 3.51 | 3.61 | 3.72 |
| | 200 | 3.28 | 3.40 | 3.51 | 3.62 | 3.72 |
| | Bulk | 1.31 | 1.36 | 1.41 | 1.46 | 1.50 |
| $V_t$ ($10^5$cm/s) | 10 | 1.33 | 1.38 | 1.42 | 1.47 | 1.51 |
| | 30 | 1.34 | 1.38 | 1.43 | 1.48 | 1.52 |
| | 70 | 1.38 | 1.39 | 1.43 | 1.48 | 1.52 |
| | 200 | 3.21 | 3.34 | 3.46 | 3.57 | 3.68 |
| | Bulk | 3.25 | 3.37 | 3.49 | 3.60 | 3.70 |

The value of isothermal bulk modulus $B_T$ of W in bulk material form at $T$ = 300K, $P$ = 0 calculated by SMM is in good agreement with experiment results shown in [8-10] and better than other calculations in [16] (see Table 5).

Table 5. $K$ of bulk W at $T$ = 300K, $P$ = 0 calculated by SMM, LDA [5], TB [5] and from EXPT [11, 16, 19]

| Method | SMM | EXPT [8-10] | LDA [16] | TB [16] |
|---|---|---|---|---|
| $K$($10^{10}$Pa) | 314 | 323 | 333 | 319 |

(LDA is the calculated result in the approximation of local density and TB is the calculation by tight-binding method).

The values of nearest neighbor distance $a$ and elastic moduli $E_Y$, $G$, $K$ of W in bulk material form at $T$ = 300K, $P$ = 0 calculated by SMM are in good agreement with experiment results in [21, 35, 38, 39] (see Table 6).

Table 6. $a$, $E_Y$, $G$, $K$ of bulk W at $T$ = 300K, $P$ = 0 calculated by SMM and from EXPT [4, 38, 40]

| Method | $a(10^{-10}$m) EXPT [38, 40] | $E_Y(10^{10}$Pa) EXPT [38] | $K(10^{10}$Pa) EXPT [41] | $G(10^{10}$Pa) EXPT [38] |
|---|---|---|---|---|
| SMM | 2.6443 | 41.40 | 31.36 | 16.17 |
| TN[38,40, 41] | 2.7400 | 41.50 | 30.00 | 16.00 |

The values of elastic constants $C_{11}$, $C_{12}$, $C_{44}$ of W in bulk material form at $T$ = 300K, $P$ = 0 calculated by SMM are in good agreement with experiment results shown in [6, 13, 39] (see Table 7)

Table 7. $C_{11}$, $C_{12}$, $C_{44}$ of bulk W at $T$ = 300K, $P$ = 0 calculated by SMM and from EXPT [38, 40, 42]

| Method | SMM | EXPT [38] | EXPT [40] | EXPT [42] |
|---|---|---|---|---|
| $C_{11}(10^{11}$Pa) | 5.29 | 5.27 | 5.21 | 5.29 |
| $C_{12}(10^{11}$Pa) | 2.06 | 1.94 | 2.02 | 1.70 |
| $C_{44}(10^{11}$Pa) | 1.62 | 1.47 | 1.60 | 1.98 |

For bulk Au at near melting temperature, the atomic volume $V = 17.29 \times 10^{-30}$ m$^3$ calculated by SMM and $V = 17.88 \times 10^{-30}$ m$^3$ according other calculations [41]. Clearly, these calculations are consistent. The values of nearest neighbor distance $a$ and elastic moduli $E_Y$, $G$, $K$ of Au in bulk material form at $T$ = 300K, $P$ = 0 calculated by SMM are in good agreement with experiment reults shown in [35, 39, 43] (see Table 8).

Table 8. $a$, $E_Y$, $G$, $K$ of bulk Au at $T$ = 300K, $P$ = 0 calculated by SMM and from EXPT [35, 39, 43]

| Method | $a(10^{-10}$m) EXPT [39, 43] | $E(10^{10}$Pa) EXPT [35] | $K(10^{10}$Pa) EXPT [35] | $G(10^{10}$Pa) EXPT [35] |
|---|---|---|---|---|
| SMM | 2.8454 | 8.96 | 14.94 | 3.20 |
| EXPT [35,39,43] | 2.8838 | 8.91 | 16.70 | 3.10 |

The values of elastic constants $C_{11}$, $C_{12}$, $C_{44}$ of Au in bulk material form at $T$ = 300K, $P$ = 0 calculated by SMM are in good agreement with experiment results shown in [38, 39] (see Table 9).

Table 9. $C_{11}$, $C_{12}$, $C_{44}$ of bulk W at $T$ = 300K, $P$ = 0 calculated by SMM and from EXPT [38, 39]

| Method | SMM | EXPT [38, 39] |
|---|---|---|
| $C_{11}(10^{11}$Pa) | 1.92 | 1.92 |
| $C_{12}(10^{11}$Pa) | 1.28 | 1.63 |
| $C_{44}(10^{11}$Pa) | 0.32 | 0.42 |

We found no theoretical or experimental evidence for the dependence of Young's modulus on interstitial atom concentration for WSi and AuSi. However, for alloys close to AuSi and CuSi, the experiments in [44-46] have shown a decrease in Young's modulus and elastic constant $C_{44}$ with increasing Si atomic concentration.

## 4. Conclusion

On the basis of the model and the theory of elastic deformation and elastic wave velocity for cubic metals and cubic binary interstitial alloy's thin films builded by the SMM, we performed numerical

calculations for films W, Au, WSi and AuSi from 100 to 1,000K, from zero to 10 GPa, from zero to 5% of interstitial atom concentration and from 10 to 200 layers. At zero interstitial atom concentration, the elastic deformation and elastic wave velocity of alloy film becomes that of main metal film. The Young modulus of alloy film decreases with the increase of temperature and increases with the increase of pressure. The Young modulus of alloy film decreases with interstitial atom concentration for film WSi and increases with interstitial atom concentration for film AuSi. As the number of layers increases until about 200 layers (at 35 nm thickness for Au and AuSi and at 30 nm for W and WSi), the elastic deformation and elastic wave velocity of alloy film approaches the values of bulk material. SMM calculations for nearest neighbor distance and elastic deformation and elastic wave velocity for bulk Au are in good agreement with the reults obtained by experiments and other calculations. Numerical results without comparative data are new results and are a reference source for prediction and experimental orientation in the future.

Funding Declaration: No funding

Competing Interest Declaration: No competing interest

## References

[1] N. Q. Hoc, B. D. Tinh, N. D. Hien, Elastic Moduli and Elastic Constants of Interstitial Alloy AuCuSi with FCC Structure under Pressure, High Temperature Materials and Processes, Vol. 38, 2019, pp. 264-272, https:// doi.org/10.1515/htmp-2018-0027.

[2] N. Q. Hoc, N. T. Hoa, N. D. Hien, D. Q. Thang, Study on Nonlinear Deformation of Binary Interstitial Alloy with BCC Structure under Pressure, HNUE Journal of Science, Natural Sciences, Vol. 63, No. 6, 2018, pp. 57-65, https://doi.org/10.18173/2354-1059.2018-0029.

[3] N. Q. Hoc, N. D. Hien, D. Q. Thang, Elastic Deformation of Alloy AuSi with BCC Structure under Pressure, HNUE Journal of Science, Natural Sciences, Vol. 63, No. 6, 2018, pp. 74-83, https://doi.org/10.18173/2354-1059.2018-0031.

[4] N. Q. Hoc, T. D. Cuong, N. D. Hien, Study on Elastic Deformation of Interstitial Alloy FeC with BCC Structure under Pressure, VNU Journal of Science: Mathematics-Physics, Vol. 35, No. 1, 2019, pp. 1-12, https://doi.org/10.25073/2588-1124/vnumap.4293.

[5] N. Q. Hoc, N. D. Hien, T. D. Nam, V. L.Thanh, Study on Elastic Deformation of Stainess Steel under Pressure, HNUE Journal of Science, Natural Sciences, Vol. 66, No. 2, 2021, pp. 83-99, https://doi.org/10.18173/2354-1059.2021-0031.

[6] B. D. Tinh, N. Q. Hoc, D. Q. Vinh, T. D. Cuong, N. D. Hien, Thermodynamic and Elastic Properties of Interstitial Alloy FeC with BCC Structure at Zero Pressure, Advanced Materials Science and Engineering, Vol. 2018, 2018, Article No. 5251741, https://doi.org/10.1155/2018/5251741.

[7] B. Wess, V. Groger, G. Khatibi, A. Kotas, P. Zimprich, R. Stickler, B. Zagar, Sensors and Actuactors A- Physical, Vol. 99, No. 1-2, 2002, pp. 172-182, https://doi.org/10.1016/S0924-4247(01)00877-9.

[8] V. V. Hung, D. D. Phuong, N. T. Hoa, H. K. Hieu, Theoretical Investigation of the Thermodynamic Properties of Metallic Thin Films, Thin Solid Film, Vol. 583, 2015, pp.7-12, https://doi.org/10.1016/j.tsf.2015.03.040

[9] V. V. Hung, D. D. Phuong, N. T. Hoa, Investigation of Thermodynamic Properties of Metal Thin Film by Statistical Moment Method, Communications in Physics, Vol. 23, No. 4, 2013, pp. 301-311, https://doi.org/10.15625/0868-3166/23/4/3351.

[10] V. V. Hung, D. D. Phuong, N. T. Hoa, Thermodynamic Properties of Free Standing Thin Metal Films Investigated by Using Statistical Moment Method: Temperature and Pressure Dependence, Communications in Physics, Vol. 24, No. 2, 2014, pp.177-191, https:// doi.org/10.15625/0868-3166/24/2/3731.

[11] H. Huang, F. Spaepen, Tensile Testing of Free-standing Cu, Ag and Al Thin Films and Ag/Cu Multilayers, Acta Materialia, Vol. 48, No. 12, 2000, pp.3261-3269, https://doi.org/10.1016/S1359-6454(00)00128-2.

[12] R. Knepper, S. P. Baker, Coefficients of Thermal Expansion and Biaxial Elastic Modulus of β Phase Tantalum Thin Films, Applied Physics Letters, Vol. 90, No. 18, 2007, Article No. 181908, https:// doi.org/10.1063/1.2734468.

[13] A. R. Vaz, M. C. Salvadori, M. Cattani, Journal of Metallic Nano Materials, Vol. 20-21, 2004, pp. 758-762, https:// doi.org/10.4028/www.scientific.net/JMNM.20-21.758.

[14] B. Wess**,** V. Groger, G. Khatibi, A. Kotas, P. Zimprich, R. Stickler, B. Zagar, Sensors and Actuactors A- Physical, Vol. 99, No. 1-2, 2002, pp. 172-182, https://doi.org/10.1016/S0924-4247(01)00877-9.

[15] Y. Kuru, M. Wohlschlogel, U. Welzel, E. J. Mittemeijer, Coefficients of Thermal Expansion of Thin Metal Films Investigated by Non-ambient X-ray Diffraction Stress Analysis, Surface and Coating Technology, Vol. 202, No. 11, 2008, pp.2306-2309, https://doi.org/10.1016/j.surfcoat.2007.08.002.

[16] D. Fuks, S. Dorfman, Y. F. Zhukovskii, E. A. Kotomin, A. M. Stoneham, Theory of the Growth Mode for a Thin Metallic Film on an Insulating Substrate, Surface Science, Vol. 499, No. 1, 2002, pp. 24-40, https://doi.org/10.1016/S0039-6028(01)01692-2.

[17] V. V. Hung, Statistical Moment Method in Studying Elastic and Thermodynamic Properties of Crystals, HNUE Publishing House, Hanoi, 2009 (in Vietmamese).

[18] A. J. Kalkman, G. C. Verbruggen, A. M. Janssen, Young's Modulus Measurements and Grain Boundary Sliding in Free-standing Thin Metal Films, Applied Physics Letters, Vol. 78, No. 18, 2001, pp. 2673-2675, https:// doi.org/10.1063/1.1367896.

[19] D. Errandonea, B. Schwager, R. Ditz, C. Gessmann, R. Boehler, M. Ross, Systematics of Transition-metal Melting, Physical Review B, Vol. 63, No. 13, 2001, Article No. 132104, https://doi.org/10.1103/PhysRevB. 63. 132104.

[20] R. D. Nyilas, S. Frank, R. Spolenak, Revealing Plastic Deformation Mechanisms in Polycrystalline Thin Films with Synchrotron XRD, JOM: The Journal of the Minerals, Metals & Materials Society, Vol. 62, No. 12, 2010, pp. 44-51, https://doi.org/10.1007/s11837-010-0179-3.

[21] N. Tang, V. V. Hung, Investigation of the Thermodynamic Properties of Anharmonic Crystals by the Momentum Method. I. General Results for Face-Centred Cubic Crystals, Physica Status Solidi (b), Vol. 149, No. 2, 1988, pp. 511-519, https://doi.org/10.1002/pssb.2221490212.

[22] D. R. Olsen, H. M. Berg, Journal of Applied Physics, Vol. 44, 1973, pp. 314-324, https://doi.org/10.1063/1.1661879.

[23] J. Tobon, C. P. S. Giraldo, H. Sanchez, Manufacture of Au-Si Alloys for Use in the Soldering of Gold Alloys, Welding International, Vol. 29, No. 8, 2015, pp. 594-599, https://doi.org/10.1080/09507116.2014.932986.

[24] T. Cagın, Thermal and Mechanical Properties of some fcc Transition Metals, Physical Review B, Vol. 59, No. 5, 1999, pp. 3468-3473, https://doi.org/ 10.1103/PhysRevB.59.3468.

[25] W. Li, H. Kou, X. Zhang, J. Ma, J. Li, P. Geng, X. Wu, L. Chen, D. Fang, Temperature-dependent Elastic Modulus Model for Metallic Bulk Materials, Mechanics of Materials, Vol. 139, 2019, Article No. 103194, https://doi.org/10.1016/j.mechmat.2019.103194.

[26] F. F. Zahroh, I. Sugihartono, E. D. Safitri, Young's Modulus Calculation of Some Metals Using Molecular Dynamics Method Based on the Morse Potential, Computational and Experimental Research in Materials and Renewable Energy (CERiMRE), Vol. 2, No. 1, 2019, pp.19-34, https://doi.org/10.19184/cerimre.v2i1.20557.

[27] Y. A. Chang, L. Himmel, Temperature Dependence of the Elastic Constants of Cu, Ag, and Au above Room Temperature, Journal of Applied Physics, Vol. 37, No. 9, 1966, pp. 3567-3572, https:// doi.org/10.1063/1.1708903.

[28] E. Güler, M. Güler, Geometry Optimization Calculations for the Elasticity of Gold at High Pressure, Advances in Materials Science and Engineering, Vol. 2013, 2023, Article No. 525673, https://doi.org/10.1155/2013/525673.

[29] M. Matsui, High Temperature and High Pressure Equation of State of Gold, Journal of Physics, Vol. 215, No. 1, 2010, Article No. 012197, https://doi.org/10.1088/1742-6596/215/1/012197.

[30] M. Yokoo, N. Kawai, K. G. Nakamura, K. I. Kondo, Y. Tange, T. Tsuchiya, Ultrahigh-pressure Scales for Gold and Platinum ai Pressures up to 550 GPa, Physical Review B, Vol. 80, 2009, Article No. 104114, https://doi.org/10.1103/PhysRevB.80.104114.

[31] S. N. Biswas, P. Van't Klooster, N. J. Trappeniers, Effect of Pressure on the Elastic Constants of Noble Metals from -196 to +25 $^{o}$C and up to 2500 bar: II. Silver and Gold, Physica B+C, Vol. 103, No. 2-3, 1981, pp. 235-246, https:// doi.org/10.1016/0378-4363(81)90127-3.

[32] T. S. Duffy, G. Shen, D. L. Heinz, J. Shu, Y. Ma, H. K. Mao, R. J. Hemley, A. K. Singh, Lattice Strains in Gold and Rhenium under Nonhydrostatic Compression to 37 GPa, Physical Review B, Vol. 60, No. 22, 1999, pp. 15063-15073, https://doi.org/10.1103/PhysRevB.60.15063.

[33] Y. Hiki, A. V. Granato, Anharmonicity in Noble Metals; Higher Order Elastic Constants, Physical Review, Vol. 144, No. 2, 1966, pp.411-419, https:// doi.org/10.1103/PhysRev.144.411.

[34] T. Tsuchiya, K. Kawamura, Ab Initio Study of Pressure Effect on Elastic Properties of Crystalline Au, Journal of Chemical Physics, Vol. 116, No. 5, 2022, pp.2121-2124, https:// doi.org/10.1063/1.1429643.

[35] N. Tang, V. V. Hung, Thermodynamic Properties of the Crystals at Various Pressures, Physica Status Solidi (b), Vol. 162, No. 2, 1990, pp. 371-377, https://doi.org/10.1002/pssb.2221620206.

[36] N. T. Hoa, N. Q. Hoc, H. X. Dat, Study on the Thermodynamic Properties of Thin Film of FCC Interstitial Alloy AuSi at Zero Pressure Using the Statistical Moment Method, Physics, Vol. 5, 2023, pp. 59-68, https://doi.org/10.3390/physics5010005.

[37] M. N. Magomedov, Calculation of Debye Temperature and Gruneisen Parameter, Journal of Physical Chemistry, Vol. 61, No. 4, 1987, pp. 1003-1009 (in Russian).

[38] L. V. Tikhonov, G. Y. Koponenko, Mechanical Properties of Metals and Alloys, Nauka-Dumka, Kiev, 1986 (in Russian).

[39] N. K. Xuong, Colour Metal Material, Science and Technique Publishing House, Hanoi, 2003 (in Vietnamese).

[40] M. J. Mehl, Pressure Dependence of the Elastic Moduli in Aluminum-rich Al-Li Compounds, Physical Review.B, Vol. 47, No. 5, 1993, pp. 2493, https://doi.org/10.1103/PhysRevB.47.2493.

[41] R. L. David, CRC Handbook of Chemistry and Physics, 86$^{th}$ Ed., Taylor & Francis, Boca Raton, London-New York-Singapore, 2005.

[42] L. Burakovsky, C. W. Greeff, D. L. Preston, Analytic Model of the Shear Modulus at All Temperatures and Densities, Physical Review B, Vol. 67, No. 9, 2003, Article No. 094107, https://doi.org/10.1103/PhysRevB.67.094107.

[43] M. J. Mehl, D. A. Papacnstantopoulos, Applications of a Tight-binding Total-energy Method for Transtion and Noble Metals: Elastic Constants, Vaccancies, and Surfaces of Monatomic Metals, Physical Review B, Vol. 54, No. 7, 1996, pp. 4519, https://doi.org/10.1103/PhysRevB.54.4519.

[44] H. M. Ledbetter, E. R. Naimon, Relationship between Single-crystal and Polycrystal Elastic Constants, Journal of Applied Physics, Vol. 45, 1974, pp.66-69, https://doi.org/10.1063/1.1663019.

[45] S. Santra, H. Dong, T. Laurila, A. Paul, Role of Different Factors Affecting Interdiffusion in Cu(Ga) and Cu(Si) Solid Solutions, The Royal Society A, Vol. 470, 2014, Article No. 20130464, https:// doi.org/10.1098/rspa.2013.0464.

[46] C. S. Smith, J. W. Burns, The Elastic Constants of Cu-4 Percent Si, Journal of Applied Physics, Vol. 24, No. 1, 1953, pp.15-18, https://doi.org/10.1063/1.1721124.